IEEE Photonics Journal
An IEEE Photonics Society Publication

Polarization Rotation in Silicon Waveguides: Analytical Modeling and Applications

Volume 2, Number 3, June 2010

Ivan D. Rukhlenko
Ivan L. Garanovich
Malin Premaratne, Senior Member, IEEE
Andrey A. Sukhorukov
Govind P. Agrawal, Fellow, IEEE
Yuri S. Kivshar

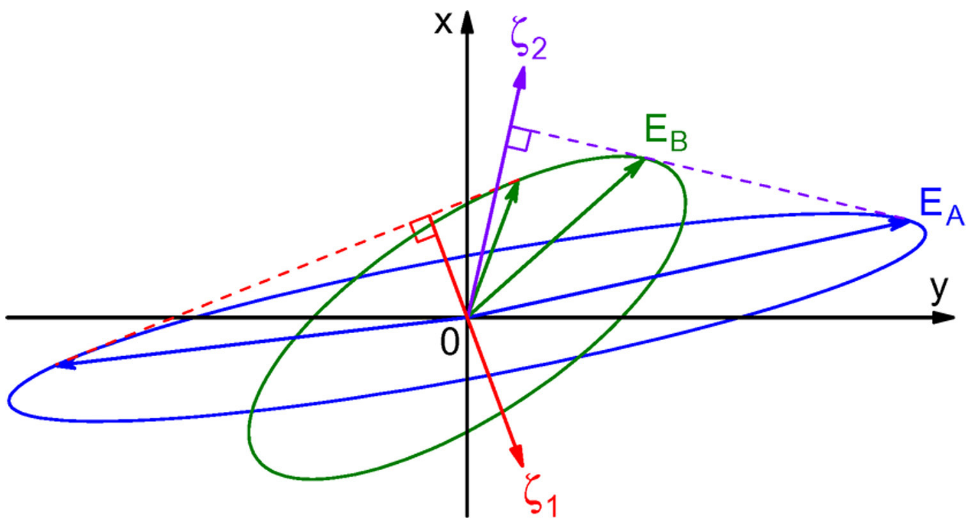

DOI: 10.1109/JPHOT.2010.2049349
1943-0655/$26.00 ©2010 IEEE

Polarization Rotation in Silicon Waveguides: Analytical Modeling and Applications

Ivan D. Rukhlenko,[1] Ivan L. Garanovich,[2]
Malin Premaratne,[1] *Senior Member, IEEE*, Andrey A. Sukhorukov,[2]
Govind P. Agrawal,[3] *Fellow, IEEE*, and Yuri S. Kivshar[2]

[1]Advanced Computing and Simulation Laboratory (AχL), Department of Electrical and Computer Systems Engineering, Monash University, Clayton, Vic. 3800, Australia
[2]Nonlinear Physics Centre, Research School of Physics and Engineering, The Australian National University, Canberra, ACT 0200, Australia
[3]Institute of Optics, University of Rochester, Rochester, NY 14627 USA

DOI: 10.1109/JPHOT.2010.2049349
1943-0655/$26.00 ©2010 IEEE

Manuscript received April 9, 2010; revised April 24, 2010; accepted April 24, 2010. Date of publication April 26, 2010; date of current version June 4, 2010. The work of I. D. Rukhlenko, M. Premaratne, and G. P. Agrawal was supported by the Australian Research Council (ARC) through its Discovery Grant scheme under Grant DP0877232. The work of G. P. Agrawal was also supported by the National Science Foundation under Award ECCS-0801772. The work of I. L. Garanovich, A. A. Sukhorukov, and Yu. S. Kivshar was supported by the ARC through its Discovery and Center of Excellence programs.
Corresponding author: I. D. Rukhlenko (e-mail: ivan.rukhlenko@eng.monash.edu.au; rukhlenko.ivan@gmail.com).

Abstract: The efficient use of optical nonlinearities in silicon is crucial for the implementation of silicon-based photonic devises. In this paper, we present an approximate analytical study of nonlinear polarization rotation in silicon-on-insulator (SOI) waveguides; the rotation is predominantly caused by the effects of self-phase modulation and cross-phase modulation, stemming from the anisotropic Kerr nonlinearity. In the first part of the paper, we analyze the transmittance of the Kerr shutter in the continuous-wave regime and address the problem of its optimization. It is essential for the generality of our conclusions that both free-carrier effects and two-photon absorption are properly accounted for in this study. We specifically show that the signal transmittance may be optimized by adjusting the waveguide length, the pump power, and the incident linear polarizations of pump and signal beams. In the second part of the paper, we examine the problem of power equalization with SOI waveguides. We validate the derived analytical solutions by comparing their predictions with the data from numerical simulations and illustrate the solutions by the examples of practical interest. The results of our work may prove useful for the design and optimization of SOI-based Kerr shutters, all-optical switches, and power equalizers.

Index Terms: Silicon nanophotonics, nonlinear optical effects in silicon, nonlinear integrated optics, Kerr effect, waveguide devices.

1. Introduction

Silicon is well known for its relatively large third-order phonon and electron nonlinearities [1]–[4], which are responsible for a variety of optical effects beneficial for device applications [5]–[9]. Apart from the pronounced nonlinear properties, two features of considerable practical value are that silicon is nearly transparent within the telecommunication window extending from 1300 to 1600 nm, and that it possesses a relatively high refractive index [3]. The latter feature enables tight confinement of optical modes inside silicon-on-insulator (SOI) waveguides and allows for the

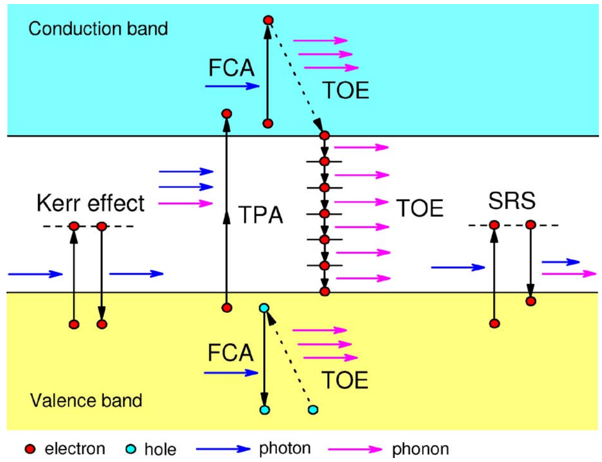

Fig. 1. Schematic of the major nonlinear effects in silicon. The process of TPA is accompanied by the absorption of a transverse optical phonon because silicon is an indirect-bandgap material.

achievement of large intensities at moderate input powers. This ensures that optical waves are efficiently guided and can be modified nonlinearly even inside a micrometer-long SOI waveguide with a lateral cross section less than 1 μm^2 [5]–[7]. Being fully compatible with the mainstream microelectronics, SOI technology is a promising candidate for on-chip integration of attractive optical functionalities and is suited for the next generation of telecommunication networks.

It is common to distinguish six major nonlinear effects associated with propagation of an arbitrary optical field through a silicon waveguide [3], [10]: the Kerr effect, two-photon absorption (TPA), free-carrier absorption (FCA), free-carrier dispersion (FCD), thermo-optic effect (TOE), and stimulated Raman scattering (SRS) (see Fig. 1). The Kerr effect is responsible for the nonlinear change in the refractive index, polarization rotation, self-phase modulation (SPM), cross-phase modulation (XPM), and four-wave mixing (FWM) processes; TPA leads to optical losses and generates free carries, which cause further FCA and change in the refractive index—both directly through FCD and mediated by TOE; finally, if the spectrum of the optical field is sufficiently broad, it is also subjected to Raman scattering, which may lead to XPM, FWM, and energy transfer between different parts of the field spectra. To appreciate the significance of these effects, one needs to take a closer look at their utilization in different photonic devices. For example, the Kerr effect is used for super-continuum generation [11]–[14], soliton formation [15], and phase modulation [16], [17]; TPA, free-carrier effects, and TOE are employed for optical modulation [18], pulse compression [19], and all-optical switching [20]–[22]; SRS is taken advantage of in Raman lasers [23]–[27], frequency converters [28]–[32], optical amplifiers [33]–[37], and modulators [38]. There is no doubt that demonstration of these functionalities, together with recent advances in fabrication of SOI wave-guides [6]–[8], will revolutionize the current photonics technology.

Although precise investigation of optical field propagation through SOI waveguides requires state-of-the-art experiments [39]–[43] and complicated numerical modeling [44]–[50], a number of valuable approximate analytical solutions has been recently obtained within the framework of a slowly varying envelope approximation [51]–[56]. Some of the analytical solutions and tools are thoroughly reviewed in Ref. [10]. With the present paper, we continue our work on analytic investigation of nonlinear optical phenomena in SOI waveguides, which proved to be useful for gaining deeper insight into nonlinear optics of silicon and silicon-based device optimization. We theoretically analyze nonlinear polarization rotation due to the Kerr-induced SPM and XPM, which may be harnessed to equalize or switch optical powers. We derive analytical expressions for transmittance of the Kerr shutter and power equalizer operating in the continuous-wave (CW) regime and use them to optimize the transmittance.

2. Coupled-Amplitude Propagation Equations

To study nonlinear polarization rotation in silicon waveguides, we consider two CW optical beams at frequencies ω_A and ω_B. The electric field of the vth beam ($v = A, B$), characterized by the lateral mode profile $F(x, y)$, can be written in the form of complex expansion

$$\mathbf{E}_v(\mathbf{r}, t) = \varpi F(x, y) \sum_{j=x,y} \mathbf{e}_j v_j(z) \exp\left[i(\beta_{vj} z - \omega_v t)\right] + \text{c.c.},$$

where $\varpi = (\mu_0/\varepsilon_0)^{1/4}(n_x + n_y)^{-1/2}$; μ_0 and ε_0 are the permittivity and permeability of vacuum; n_j and $\mathbf{e}_j$ are the linear refractive index and a unit vector in the jth direction; $v_j(z)$ is jth-component amplitude of the vth field (in units of the square root of intensity); $\beta_{vj} = k_v n_j$; $k_v = \omega_v/c_0$; and c_0 is the velocity of light. We assume for simplicity that the frequencies of the two beams are so close to each other that the shape and the effective index of the mode are nearly the same for both beams.

The evolution of amplitudes $v_j(z) = \{A_x, A_y, B_x, B_y\}$ inside the SOI waveguide of constant cross section is governed by the coupled nonlinear differential equations [1], [3], [49]

$$\frac{1}{A_x}\frac{dA_x}{dz} = H(z) - \left(\frac{\beta}{2} - i\gamma\right)\left[a\left(|A_x|^2 + 2|B_x|^2\right) + c\left(|A_y|^2 + 2|B_y|^2\right) + cA_y^2 \frac{A_x^*}{A_x} e^{-2i\Delta\beta_A z}\right], \tag{1a}$$

$$\frac{1}{A_y}\frac{dA_y}{dz} = H(z) - \left(\frac{\beta}{2} - i\gamma\right)\left[b\left(|A_y|^2 + 2|B_y|^2\right) + c\left(|A_x|^2 + 2|B_x|^2\right) + cA_x^2 \frac{A_y^*}{A_y} e^{2i\Delta\beta_A z}\right], \tag{1b}$$

$$\frac{1}{B_x}\frac{dB_x}{dz} = H(z) - \left(\frac{\beta}{2} - i\gamma\right)\left[a\left(|B_x|^2 + 2|A_x|^2\right) + c\left(|B_y|^2 + 2|A_y|^2\right) + cB_y^2 \frac{B_x^*}{B_x} e^{-2i\Delta\beta_B z}\right], \tag{1c}$$

$$\frac{1}{B_y}\frac{dB_y}{dz} = H(z) - \left(\frac{\beta}{2} - i\gamma\right)\left[b\left(|B_y|^2 + 2|A_y|^2\right) + c\left(|B_x|^2 + 2|A_x|^2\right) + cB_x^2 \frac{B_y^*}{B_y} e^{2i\Delta\beta_B z}\right], \tag{1d}$$

where the function $H(z)$ includes linear losses through the absorption coefficient α, and the free-carrier effects through the coefficients ξ_i and ξ_r,

$$H(z) = -\frac{\alpha}{2} - \left(\frac{\xi_r}{2} + i\xi_i\right)\left[\left(|A_x|^2 + |A_y|^2\right)^2 + \left(|B_x|^2 + |B_y|^2\right)^2 + 4\left(|A_x|^2 + |A_y|^2\right)\left(|B_x|^2 + |B_y|^2\right)\right].$$

In the second terms on the right-hand side of (1), the constant β accounts for TPA, while the coefficient $\gamma = kn_2$, with $k = \omega/c_0$, $\omega = (\omega_A + \omega_B)/2$, and n_2 being the nonlinear Kerr parameter, governs the Kerr effect. The parameters $\xi_r = \sigma_r (k_0/k)^2 \tau_c \beta/(2\hbar\omega)$ and $\xi_i = \sigma_i (k_0/k)^2 \tau_c \beta/(2\hbar c_0)$ describe the effects of FCA and FCD, whose strength is determined by the effective free-carrier lifetime τ_c; $\sigma_r = 1.45 \times 10^{-21}$ m^2, $\sigma_i = 5.3 \times 10^{-27}$ m^3, and $2\pi/k_0 = 1.55$ μm [3].

The coefficients a, b, and c describe anisotropy of the Kerr effect and TPA; their values depend on the orientation of the crystallographic axes in the SOI waveguide. If the waveguide is fabricated along the [010] or [001] directions, then the electronic response is isotropic with $a = b = 1$, $c = \rho/3$, and $\rho \approx 1.27$. Anisotropy arises for SOI waveguides fabricated along the [0$\bar{1}$1] direction; in this case $a = 1$, $b = (1 + \rho)/2$, and $c = \rho/3$, for the same value of anisotropic factor ρ [53]. The wave vector mismatch between field components v_x and v_y, $\Delta\beta_v = k_v \Delta n$ is proportional to the linear modal birefringence of the waveguide, $\Delta n = n_x - n_y$. It should be also noted that, even though TOE generally induces the highest nonlinear phase shifts [51], [52], it is neglected in our study because of its isotropic nature. For the same reason, the effect of FCD also has nearly no impact on polarization rotation.

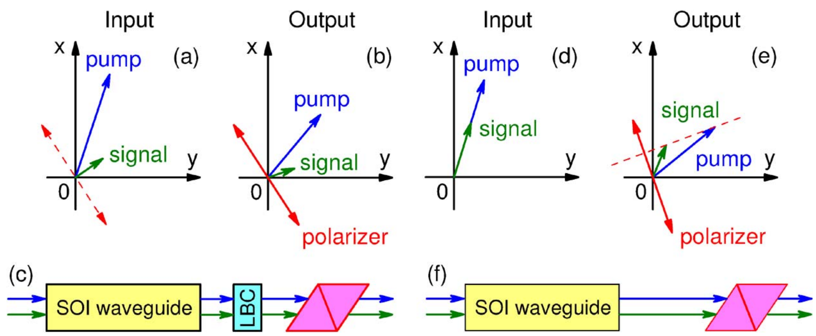

Fig. 2. Operation scheme of the (a)–(c) Kerr shutter and (d)–(f) power equalizer, based on the XPM-induced polarization rotation in SOI waveguides with principal axes x and y. Both the pump and the signal are assumed to be linearly polarized; LBC denotes the linear birefringence compensator.

In order to distinguish between different polarizations, we can use an optical polarizer (analyzer). If the orientation of the polarizer at the end of an SOI waveguide of length L is determined by the unit vector $\mathbf{e}_p = \mathbf{e}_x \cos\zeta + \mathbf{e}_y \sin\zeta$, the intensity of the transmitted beam v is given by

$$\begin{aligned} I_v(\zeta) &= \frac{\omega_v}{2\pi} \iint dxdy \int_0^{2\pi/\omega_v} dt \left(\frac{\mathbf{E}_v(\mathbf{r}, t) \cdot \mathbf{e}_p}{\varpi} \right)^2 \Bigg|_{z=L} \\ &= |v_x(L)|^2 \cos^2\zeta + |v_y(L)|^2 \sin^2\zeta + |v_x(L) v_y(L)| \sin 2\zeta \cos\Delta\phi_v, \end{aligned} \tag{2}$$

where $\Delta\phi_v = k_v \Delta n L + \mathrm{Arg}[v_x(L)/v_y(L)]$ is the total phase shift between x- and y-electric-field components of the vth wave, and we assume that the amplitudes are normalized according to $\iint F^2(x, y) dxdy = 1/2$.

3. Optical Switching

In many practical situations, one of two beams, called the signal, is so weak that it does not cause nonlinear effects. Its polarization can be rotated via XPM in the presence of another strong beam called the pump. With this effect, one can construct an all-optical Kerr shutter that can be switched-open for ultrashort durations ($\sim$1 ps) using short pump pulses at repetition rates of up to $\omega_{\max} = \tau_c^{-1}$ [53]. Such a Kerr shutter has recently been demonstrated [57].

The general scheme of the Kerr shutter and its operating principle are illustrated in Fig. 2(a)–(c). Without the pump, the signal beam is blocked by an appropriately adjusted polarizer at the end of the waveguide, as shown in Fig. 2(a). This can be achieved, provided that the linear birefringence of silicon is compensated, and the signal is linearly polarized after passing the waveguide. In the presence of the pump, the polarization of the signal becomes elliptic due to XPM, resulting in its partial transmittance through the polarizer [see Fig. 2(b)]. Since the magnitude of XPM depends on optical power, the transmission of the Kerr shutter is governed by the pump intensity.

3.1. Simplified Propagation Equations

The operation of the Kerr shutter is described by system (1), which may be substantially simplified since the pump is much stronger than the signal. Neglecting the signal-induced XPM and signal-induced nonlinear losses, we obtain from (1a) and (1b) the following equations for the pump amplitudes:

$$\frac{1}{A_x}\frac{dA_x}{dz} = -\frac{\alpha}{2} - \left(\frac{\xi_r}{2} + i\xi_i\right) I_A^2 - \left(\frac{\beta}{2} - i\gamma\right)\left(a|A_x|^2 + c|A_y|^2 + cA_y^2 \frac{A_x^*}{A_x} e^{-2i\Delta\beta_A z}\right), \tag{3a}$$

$$\frac{1}{A_y}\frac{dA_y}{dz} = -\frac{\alpha}{2} - \left(\frac{\xi_r}{2} + i\xi_i\right) I_A^2 - \left(\frac{\beta}{2} - i\gamma\right)\left(b|A_y|^2 + c|A_x|^2 + cA_x^2 \frac{A_y^*}{A_y} e^{2i\Delta\beta_A z}\right), \tag{3b}$$

where $I_A = |A_x|^2 + |A_y|^2$ is the pump intensity.

Similarly, after ignoring the signal-induced nonlinear losses and the effect of SPM in the equations for signal, we obtain

$$\frac{1}{B_x}\frac{dB_x}{dz} = -\frac{\alpha}{2} - \left(\frac{\xi_r}{2} + i\xi_i\right) I_A^2 - (\beta - 2i\gamma)\left(a|A_x|^2 + c|A_y|^2\right), \tag{4a}$$

$$\frac{1}{B_y}\frac{dB_y}{dz} = -\frac{\alpha}{2} - \left(\frac{\xi_r}{2} + i\xi_i\right) I_A^2 - (\beta - 2i\gamma)\left(b|A_y|^2 + c|A_x|^2\right). \tag{4b}$$

Let us denote by $\vartheta = \tan^{-1}|B_x(0)/B_y(0)|$ the angle between the x-axis and the incident linear polarization of signal. To block the signal in the absence of pump and linear birefringence, the polarizer axis should be perpendicular to the direction specified by ϑ, i.e., $\zeta = \vartheta \pm \pi/2$. Then, using (2) and taking into account that the intensity-independent phase shift of signal is compensated at the output (or input) end of the waveguide [see Fig. 2(c)], we arrive at the signal transmittance in the form

$$T = \frac{|B_x(L)|^2\sin^2\vartheta + |B_y(L)|^2\cos^2\vartheta - |B_x(L)B_y(L)|\sin 2\vartheta\cos\Delta\phi_{\mathrm{NL}}}{|B_x(0)|^2 + |B_y(0)|^2}, \tag{5}$$

where $\Delta\phi_{\mathrm{NL}} = \mathrm{Arg}[B_x(L)/B_y(L)]$ is the nonlinear phase shift between the x- and y-amplitudes of signal at the end of the waveguide. To find the value of T using this equation, one needs to solve (3) and (4) with boundary conditions $I_v(0) = I_{v0}$.

3.2. Approximate Analytical Solution

To describe the process of optical switching analytically, we ignore the last terms in (3). These terms are responsible for degenerated FWM between the polarization components of the pump [46], and our approximation is justified by the agreement with the full numerical modeling (see Section 3.3). Neglecting the impact of TPA on the attenuation of pump, we obtain the following differential equations for the intensities $I_{vj} = |v_j|^2$:

$$\frac{1}{I_{Aj}}\frac{dI_{Aj}}{dz} \approx -\alpha - \xi_r I_A^2,$$

$$\frac{1}{I_{Bx}}\frac{dI_{Bx}}{dz} \approx -\alpha - \xi_r I_A^2 - 2\beta(aI_{Ax} + cI_{Ay}),$$

$$\frac{1}{I_{By}}\frac{dI_{By}}{dz} \approx -\alpha - \xi_r I_A^2 - 2\beta(bI_{Ay} + cI_{Ax}).$$

The solution of these equations at $z = L$ is readily found to be

$$I_{Ax}(L) = I_{A0}f(L)\cos^2\varphi, \quad I_{Ay}(L) = I_{A0}f(L)\sin^2\varphi, \tag{6a}$$

$$I_{Bx}(L) = I_{B0}f(L)\exp\left[-2\beta(a\cos^2\varphi + c\sin^2\varphi)I_{A0}L_{\mathrm{eff}}\right]\cos^2\vartheta, \tag{6b}$$

$$I_{By}(L) = I_{B0}f(L)\exp\left[-2\beta(b\sin^2\varphi + c\cos^2\varphi)I_{A0}L_{\mathrm{eff}}\right]\sin^2\vartheta, \tag{6c}$$

where $\varphi = \tan^{-1}|A_x(0)/A_y(0)|$ is the angle between incident linear polarization of the pump and the x-axis; the function $f(z)$ and the constant L_{eff} are defined as

$$f(z) = \frac{\exp(-\alpha z)}{\sqrt{1 + I_{A0}^2(\xi_r/\alpha)[1 - \exp(-2\alpha z)]}}, \quad L_{\mathrm{eff}} = \frac{\tan^{-1}\left[I_{A0}\sqrt{\xi_r/\alpha}\right] - \tan^{-1}\left[I_{A0}f(L)\sqrt{\xi_r/\alpha}\right]}{I_{A0}\sqrt{\alpha\xi_r}}. \tag{7}$$

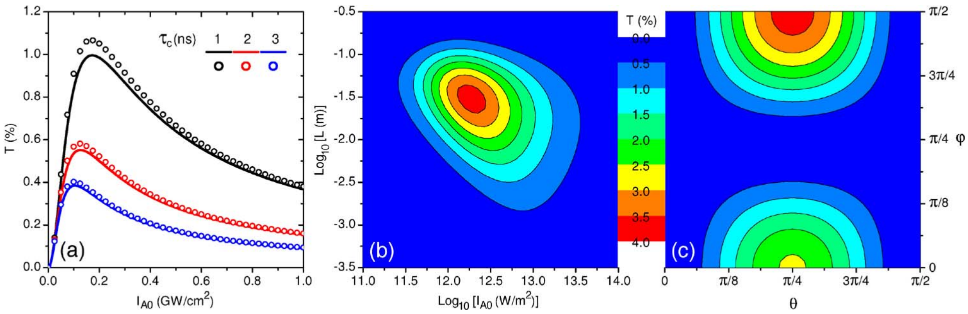

Fig. 3. (a) Comparison of approximate analytical solution given in (8) (solid curves) with the transmittance calculated numerically using (3) and (4) (open circles) for free-carrier lifetimes of 1, 2, and 3 ns; $L = 5$ cm, $I_{B0} = 1$ MW/cm^2, $\vartheta = \pi/4$, and $\varphi = \pi/3$. (b) and (c) Contour plots of signal transmittance in the (L, I_{A0}) and (ϑ, φ) domains for $\tau_c = 1$ ns; (b) $\vartheta = \pi/4$ and $\varphi = \pi/2$; (c) $L = 3.2$ cm and $I_{A0} = 178$ MW/cm^2. Other parameters are specified in the text.

Physically speaking, $f(z)$ characterizes the decrease of intensities due to linear absorption and FCA, while L_{eff} gives the effective length of the waveguide [10], [51], [52] "seen" by the Kerr effect. The nonlinear phase shift $\Delta\phi_{\mathrm{NL}}$ satisfies the equation

$$\frac{d(\Delta\phi_{\mathrm{NL}})}{dz} = \mathrm{Im}\left(\frac{1}{B_x}\frac{dB_x}{dz} - \frac{1}{B_y}\frac{dB_y}{dz}\right) = 2\gamma\left[(a-c)\cos^2\varphi - (b-c)\sin^2\varphi\right] I_{A0} f(z),$$

the solution of which at $z = L$ is

$$\Delta\phi_{\mathrm{NL}} = 2\gamma\left[(a-c)\cos^2\varphi - (b-c)\sin^2\varphi\right] I_{A0} L_{\mathrm{eff}}.$$

By substituting (6b) and (6c) into (5), we obtain

$$\begin{aligned} T = f(L)\sin^2\vartheta\cos^2\vartheta\{&\exp\left[-2\beta(a\cos^2\varphi + c\sin^2\varphi)I_{A0}L_{\mathrm{eff}}\right] \\ &+ \exp\left[-2\beta(b\sin^2\varphi + c\cos^2\varphi)I_{A0}L_{\mathrm{eff}}\right] \\ &- 2\exp\left[-\beta(a\cos^2\varphi + b\sin^2\varphi + c)I_{A0}L_{\mathrm{eff}}\right]\cos\Delta\phi_{\mathrm{NL}}\}. \end{aligned} \tag{8}$$

It is easy to see that, in the absence of linear losses $(\alpha = 0)$, TPA $(\beta = 0)$, FCA $(\xi_r = 0)$, and anisotropy $(a = b)$, the preceding result is reduced to

$$T = \sin^2[\gamma(a-c)\cos(2\varphi)I_{A0}L]\sin^2 2\vartheta. \tag{9}$$

This equation is similar in structure to the well known formula, describing the net transmission of optical pulse through birefringent fibers [46], [58]. Interestingly, even though (8) is a much more complex function of φ as compared to (9), they both have a maximum at $\varphi = 0$ and $\varphi = \pi/2$. The value of T at $\varphi = 0$ may be greater or lesser than the value of T at $\varphi = \pi/2$, depending on the input pump intensity and the waveguide length. Since the function (8) also have a maximum at $\vartheta = \pi/4$, the optimal transmittance is achieved for signal that equally excites TE and TM modes.

3.3. Numerical Examples and Discussion

We illustrate the above analysis for SOI waveguides fabricated along the $[0\bar{1}0]$ direction, using the pump at wavelength 1.55 μm and the signal at wavelength 1.54 μm. We assume that the modal birefringence of the waveguide is $\Delta n = 1.2 \times 10^{-3}$ [59]. The other parameters' values are as follows [51], [52]: $\alpha = 1$ dB/cm, $\beta = 0.5$ cm/GW, and $n_2 = 6 \times 10^{-5}$ GW/cm^2.

Fig. 3(a) shows the signal transmittance through a 5-cm-long waveguide as a function of incident pump intensity for different free-carrier lifetimes. The analytical results shown by solid curves are verified by the numerical solution of (3) and (4), represented by opened circles. As is seen from the figure, the numerical and analytical results agree reasonably well with each other. The minor discrepancy between them does not exceed 10% for $\tau_c = 1$ ns and becomes smaller for longer free-carrier lifetimes. Thus, under typical operating conditions of the SOI-based Kerr shutter, the impact of degenerated FWM on the pump is negligible, which justifies our approximation made to obtain the solution given in (6).

The absolute values of the transmittance are small due to the strong nonlinear absorption caused by the TPA-generated free carriers. Practically, the detrimental effect of FCA cannot be substantially reduced without resort to carrier sweeping by an external electric field. It is significant, therefore, that the transmittance of the Kerr shutter may be maximized by appropriately choosing the operating intensity I_{A0}, waveguide length L, and incident linear polarization of the pump φ. The existence of the optimal pump intensity is evident from Fig. 3(a). The optimal waveguide length occurs because the transmittance is low, both for relatively short waveguides due to weak XPM, and for relatively long waveguides due to strong FCA. Since the maximum of the transmittance is reached at either $\varphi = 0$ or $\varphi = \pi/2$ (depending on the values of I_{A0} and L), the performance of the Kerr shutter can be optimized using the following steps. First, set $\varphi = 0$ and find the values of I_{A0} and L that provide the maximal value for T, $\max[T(\varphi = 0)]$. Then, using these values, calculate the transmittance at $\varphi = \pi/2$, $T(\varphi = \pi/2)$, and compare it with $\max[T(\varphi = 0)]$. If $\max[T(\varphi = 0)] > T(\varphi = \pi/2)$, then the obtained values of I_{A0}, L, and $\varphi = 0$ are optimal. Otherwise, the optimal incident polarization of pump corresponds to $\varphi = \pi/2$, and the optimal values of I_{A0} and L are those that give maximum transmittance at $\varphi = \pi/2$.

Fig. 3(b) shows the contour plot of T as a function of L and I_{A0} for $\tau_c = 1$ ns, $\vartheta = \pi/4$, and $\varphi = \pi/2$. One may see that the maximal transmittance (about 4%) is achieved for $L \approx 3.2$ cm and $I_{A0} \approx 178$ MW/cm^2. Because in this case $\max[T(\varphi = \pi/2)] > T(\varphi = 0)$ [see Fig. 3(c)], these values of I_{A0} and L are optimal for the waveguide in question.

We also note that one can construct an all-optical switch based on the considered Kerr-shutter scheme making use of an SOI waveguide, a beam splitter, and two polarizers. With proper modifications allowing for a specific design, the presented theory can be used to optimize the performance of such a Kerr switch.

4. Power Equalization

The nonlinear polarization rotation in silicon waveguides can be employed to equalize optical powers of a two-level signal [60] or of two beams. The SOI-based power equalizer consists of an SOI waveguide and an output polarizer shown in Fig. 2(f). Its operation principle can be understood by looking at schemes in Figs. 2(d) and 2(e), illustrating the case of two beams with identical linear polarizations at the input. Since the Kerr-induced birefringence depends on optical power, the polarizations of beams with different powers exhibit unequal evolution. As a result, after passing through a suitable waveguide, the powers of the beams may be matched using an appropriately rotated polarizer.

4.1. Approximate Analytical Solution

Let us first consider equalization of powers for two beams with different frequencies. Since in the waveguide of constant cross section the power and intensity of each beam are proportional, we require the equality of intensities, $I_A(\zeta) = I_B(\zeta) \equiv I(\zeta)$. Using (2), we obtain the following equation for the polarizer's angle ζ:

$$\sin^2\varphi\tan^2\zeta + q\sin 2\varphi\tan\zeta + \cos^2\varphi = 0, \tag{10}$$

where

$$q = \frac{I_{A0}\cos\Delta\phi_A - I_{B0}\cos\Delta\phi_B}{I_{A0} - I_{B0}}.$$

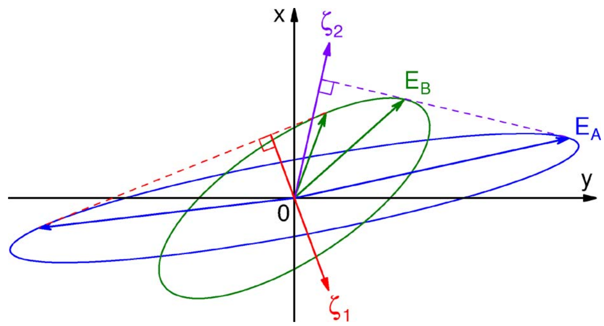

Fig. 4. Schematic representation of the two roots given in (11). The elliptically polarized beams are equally transmitted through polarizers whose axis have equal maximum projections of the electric fields E_A and E_B.

Neglecting TPA and degenerate FWM in (1), we can show that the phase shifts between the TE and TM components of the beams are given by

$$\Delta\phi_A \approx k_A \Delta n L + 2\gamma\left[(a-c)\cos^2\varphi - (b-c)\sin^2\varphi\right](I_{A0} + 2I_{B0})L_{\text{eff}}(I_\Sigma),$$
$$\Delta\phi_B \approx k_B \Delta n z + 2\gamma\left[(a-c)\cos^2\varphi - (b-c)\sin^2\varphi\right](I_{B0} + 2I_{A0})L_{\text{eff}}(I_\Sigma),$$

provided that $k_A \neq k_B$. Here, the parameter $L_{\text{eff}}(I_\Sigma)$ is given by (7) after the replacement $I_{A0} \to I_\Sigma = (I_{A0}^2 + I_{B0}^2 + 4I_{A0}I_{B0})^{1/2}$.

The solution of (10) is given by

$$\tan\zeta_{1,2} = -\frac{q \pm \sqrt{q^2-1}}{\tan\varphi}. \tag{11}$$

One can see that equalization of intensities I_{A0} and I_{B0} using SOI waveguide of a given length is only possible if they satisfy the inequality $|q| \geq 1$, which holds when I_{A0} and I_{B0} are not too far apart initially. When this is the case, there are two possible orientations of the output polarizer, specified by the angles ζ_1 and ζ_2. The existence of two solutions is illustrated in Fig. 4 graphically. If $|q| < 1$, the incident intensities cannot be equalized with a given waveguide, no matter what the value of φ is. In Fig. 4, this situation would be represented by one polarization ellipse located inside the other.

It is easy to see that the parameter q reaches infinity for equal input intensities, $I_{A0} = I_{B0}$. As this occurs, $\zeta_{1,2} = 0$, $\pi/2$, and the polarizer axis should be aligned with either x- or y-crystallographic direction. Because of different phase shifts due to linear birefringence, the intensities corresponding to these orientations are different, unless $\varphi = \pi/4$. In the latter case, $I(\zeta_1) = I(\zeta_2)$ for any allowed values of input intensities. This can be readily seen by using in (2) the consequence of (11), i.e., $\zeta_1 + \zeta_2 = \pm\pi/2$. Generally, one can show that

$$I(\zeta_1) \gtrless I(\zeta_2) \quad \text{for} \quad I_{A0} \gtrless I_{B0} \quad \text{and} \quad \varphi < \pi/4,$$
$$I(\zeta_2) \gtrless I(\zeta_1) \quad \text{for} \quad I_{A0} \gtrless I_{B0} \quad \text{and} \quad \varphi > \pi/4.$$

These inequalities imply that roots ζ_1 and ζ_2 switch their values at $I_{A0} = I_{B0}$. When $q = \pm 1$, the roots in (11) coincide and are equal to $\pm\varphi$.

In the case of one quasi-CW signal with two intensity levels, $I_{A0} \neq I_{B0}$, the phase shifts in (10) become

$$\Delta\phi_A \approx k\Delta n L + 2\gamma\left[(a-c)\cos^2\varphi - (b-c)\sin^2\varphi\right]I_{A0}L_{\text{eff}}(I_{A0}),$$
$$\Delta\phi_B \approx k\Delta n L + 2\gamma\left[(a-c)\cos^2\varphi - (b-c)\sin^2\varphi\right]I_{B0}L_{\text{eff}}(I_{B0}),$$

where $L_{\text{eff}}(I_{j0})$ is given by (7) with I_{A0} replaced by I_{j0}. In deriving these equations, we considered only the effects of SPM and neglected the last terms in (1).

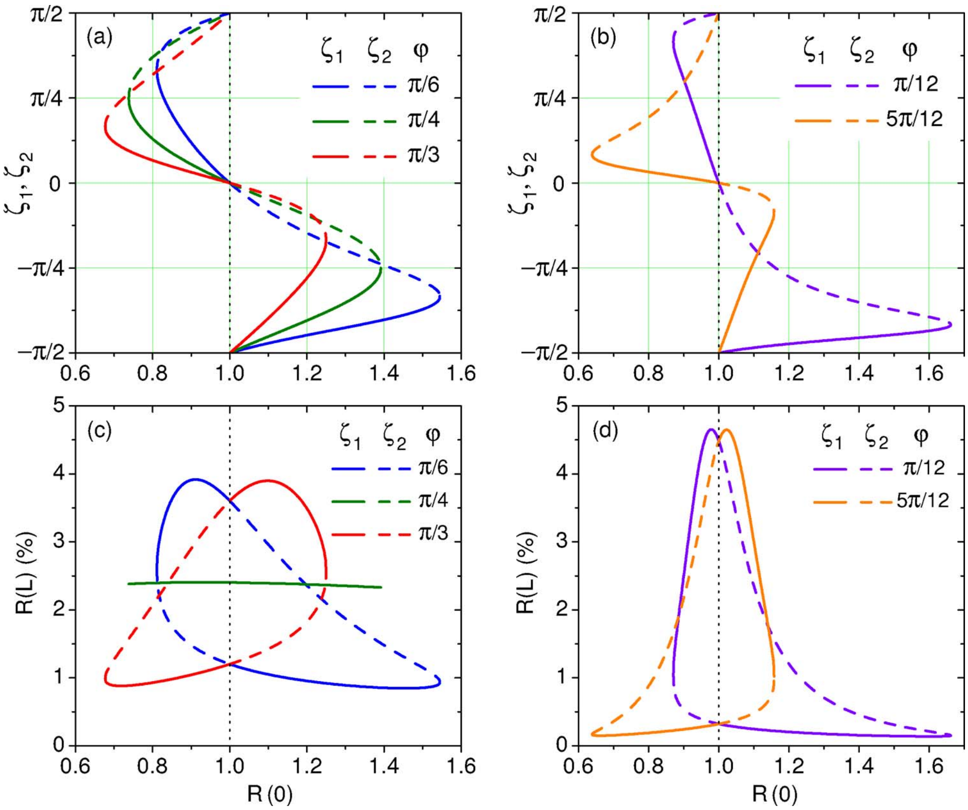

Fig. 5. Polarizer's angles, which equalize intensities of two beams passed through a 1-cm-long SOI waveguide (a) and (b), and the corresponding output intensities (c) and (d). The function $R(z) = I_{B0}(z)/I_{A0}$ with $I_{A0} = 1$ GW/cm^2, gives the ratio of input intensities for $z = 0$, and characterizes the output intensity for $z = L$. For all panels, $\tau_c = 1$ ns; the other parameters' values are the same as in Fig. 3.

It is important to note that the phase shift due to linear birefringence is the same for both power levels of a two-level signal. Since it is vastly larger than the Kerr-induced phase shift, which saturates with increasing L, not all power levels of a signal can be equalized using a silicon waveguide of given length. Moreover, some waveguides allow no power equalization; it is easy to show, however, that any two power levels may be equalized by adjusting the waveguide length by less than $\delta L = 2\pi/(k\Delta n)$. Notice that for $I_{A0} = I_{B0}$, the obtained solution predicts only two polarizer angles from an infinite set $\zeta \in [0, \pi/2]$.

4.2. Numerical Examples and Discussion

The above results allow one to identify the optimal operation conditions for silicon-based power equalizers. In the first example, we consider two optical beams at wavelengths of 1.54 and 1.55 μm, propagating through silicon waveguide with $L = 1$ cm and $\tau_c = 1$ ns. Figs. 5(a) and 5(b) show the values of angles $\zeta_{1,2}$ for five input polarizations set as $\varphi = (\pi/12)m$ $(m = 1, 2, \ldots, 5)$. The solid and dashed curves specify the directions of polarizer axis that are required for equalization of the different powers of beam B with the fixed power of beam A, $I_{A0} = 1$ GW/cm^2. Figs. 5(c) and 5(d) represent the corresponding output intensities (in the percents of intensity I_{A0}) as functions of the input intensity of beam B. It can be seen that power equalization is only possible within a certain band whose position depends on the value of φ. Whereas the range of intensities, which can be equalized, does not change significantly as φ varies from $\pi/6$ to 0 and from $\pi/3$ to $\pi/2$, the efficiency of the power equalizer (in terms of transmitted power versus input power) approaches zero at the band's boundaries for $\varphi \to 0$, $\pi/2$. It should be also noted from Fig. 5(c) that the output

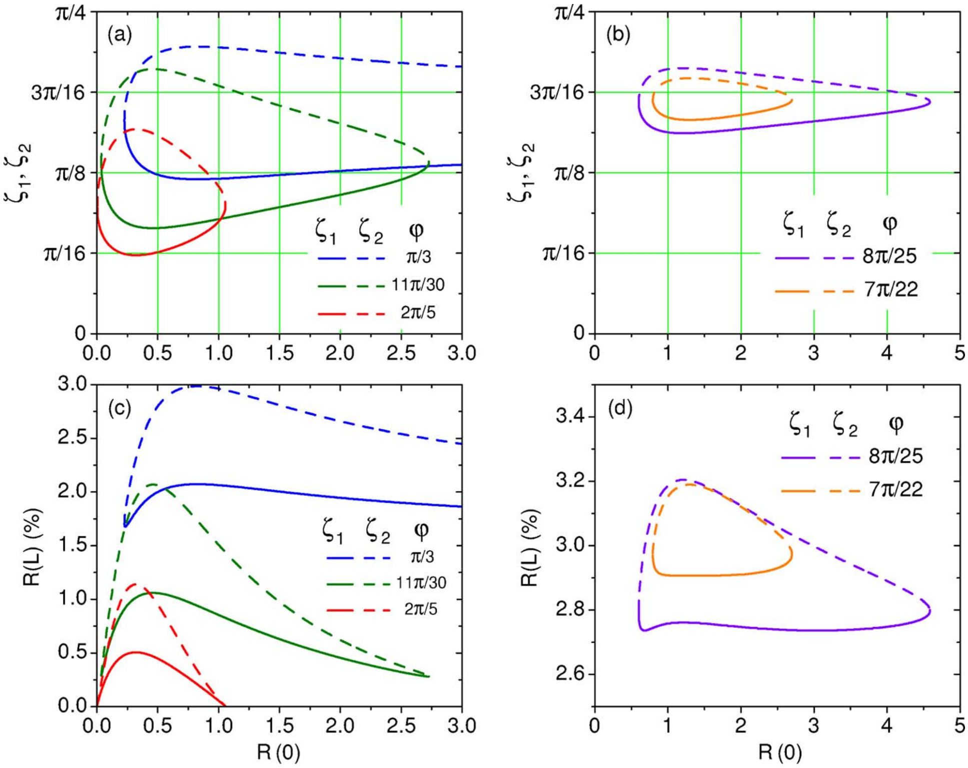

Fig. 6. Polarizer's angles, which equalize powers in a two-level signal passed through a 1-cm-long SOI waveguide (a) and (b), and the corresponding output intensities (c) and (d). The function $R(z)$ is the same as in Fig. 5. For all panels, $\tau_c = 0.1$ ns; the other parameters' values are the same as in Fig. 3.

intensity is nearly independent on I_{B0} when $\varphi = \pi/4$. Thus one can use the same waveguide for beams with different powers.

Fig. 6 shows an example of power equalization for a two-level signal at wavelength 1.55 μm. As before, one of the signal's levels has a fixed power $I_{A0} = 1$ GW/cm^2, while the power of the other level is varied. The effective free-carrier lifetime is set to 0.1 ns so that the nonlinear phase shifts are large enough to enable equalization of powers in a 1-cm-long waveguide. From this figure we see that the performance of power equalizer drastically depends on the incident polarization. For instance, one may equalize powers $I_{B0} \gg I_{A0}$ when $\varphi = \pi/3$, but no efficient equalization is possible for $I_{B0} > I_{A0}$ if φ exceeds $2\pi/5$. The range of admissible intensities I_{B0} steeply reduces with φ decreasing from $\pi/3$, and vanishes for $\varphi < 57°$ [see Figs. 6(b) and 6(d)]. From the practical standpoint, it is important that for $\varphi = \pi/3$, the polarizer's angle $\zeta_1 \approx \pi/8$ leads to almost constant equalizer efficiency of 2% in a broad range of input powers. This feature may be used to equalize powers in multilevel signals. Figs. 5 and 6 also suggest that optimization of the waveguide length, input polarization, and polarizer angle is crucial for efficient operation of silicon-based power equalizers.

We also note that, for shorter free-carrier lifetimes, power equalization is possible within a number of bands about different values of ratio I_{A0}/I_{B0}. The bands' boundaries are determined by incident intensities corresponding to $|q| = 1$. Since FCA introduces considerable losses, but FCD does not contribute to the nonlinear polarization rotation in silicon waveguides, a long free-carrier lifetime is a disadvantage for the above-discussed applications; the value of this parameter should be reduced in practice as much as possible.

5. Conclusion

In this work, we theoretically studied the phenomenon of nonlinear polarization rotation in silicon waveguides in the continuous-wave regime. Starting with the propagation equations for coupled amplitudes, we derived approximate analytical expression for the transmittance of the Kerr shutter and investigated the possibility of using silicon waveguide for equalization of optical powers. We showed that there exist an optimal waveguide length and an optimal pump power that maximize the signal transmission in the Kerr-shutter scheme. We also demonstrated that there are two possible orientations of the output polarizer that equalize powers of two beams passing through the waveguide. The performance of the Kerr shutter and the power equalizer depend on the incident linear polarizations, the effective free-carrier lifetime, and the polarizer's angle. The developed theory provides a simple, yet powerful tool for design optimization of the examined devices with respect to these parameters.

References

[1] R. M. Osgood, Jr., N. C. Panoiu, J. I. Dadap, X. Liu, X. Chen, I.-W. Hsieh, E. Dulkeith, W. M. J. Green, and Y. A. Vlasov, "Engineering nonlinearities in nanoscale optical systems: Physics and applications in dispersion-engineered silicon nanophotonic wires," *Adv. Opt. Photon.*, vol. 1, no. 1, pp. 162–235, Jan. 2009.

[2] H. K. Tsang and Y. Liu, "Nonlinear optical properties of silicon waveguides," *Semicond. Sci. Technol.*, vol. 23, no. 6, pp. 064007-1–064007-9, May 2008.

[3] Q. Lin, O. J. Painter, and G. P. Agrawal, "Nonlinear optical phenomena in silicon waveguides: Modeling and applications," *Opt. Express*, vol. 15, no. 25, pp. 16 604–16 644, Dec. 2007.

[4] M. Dinu, F. Quochi, and H. Garcia, "Third-order nonlinearities in silicon at telecom wavelengths," *Appl. Phys. Lett.*, vol. 82, no. 18, pp. 2954–2956, May 2003.

[5] M. A. Foster, A. C. Turner, M. Lipson, and A. L. Gaeta, "Nonlinear optics in photonic nanowires," *Opt. Express*, vol. 16, no. 2, pp. 1300–1320, Jan. 2008.

[6] C. Koos, L. Jacome, C. Poulton, J. Leuthold, and W. Freude, "Nonlinear silicon-on-insulator waveguides for all-optical processing," *Opt. Express*, vol. 15, no. 10, pp. 5976–5990, May 2007.

[7] B. Jalali, V. Raghunathan, D. Dimitropoulos, and O. Boyraz, "Raman-based silicon photonics," *IEEE J. Sel. Topics Quantum Electron.*, vol. 12, no. 3, pp. 412–421, May/Jun. 2006.

[8] R. A. Soref, "The past, present, and future of silicon photonics," *IEEE J. Sel. Topics Quantum Electron.*, vol. 12, no. 6, pp. 1678–1687, Nov./Dec. 2006.

[9] G. T. Reed and A. P. Knights, *Silicon Photonics: An Introduction*. Hoboken, NJ: Wiley, 2004.

[10] I. D. Rukhlenko, M. Premaratne, and G. P. Agrawal, "Nonlinear silicon photonics: Analytical tools," *IEEE J. Sel. Topics Quantum Electron.*, vol. 16, no. 1, pp. 200–215, Jan./Feb. 2010.

[11] L. Yin, Q. Lin, and G. P. Agrawal, "Soliton fission and supercontinuum generation in silicon waveguides," *Opt. Lett.*, vol. 32, no. 4, pp. 391–393, Feb. 2007.

[12] I.-W. Hsieh, X. Chen, X. Liu, J. I. Dadap, N. C. Panoiu, C. Y. Chou, F. Xia, W. M. Green, Y. A. Vlasov, and R. M. Osgood, Jr., "Supercontinuum generation in silicon photonic wires," *Opt. Express*, vol. 15, no. 23, pp. 15 242–15 249, Nov. 2007.

[13] O. Boyraz, P. Koonath, V. Raghunathan, and B. Jalali, "All-optical switching and continuum generation in silicon waveguides," *Opt. Express*, vol. 12, no. 17, pp. 4094–4102, Aug. 2004.

[14] O. Boyraz, T. Indukuri, and B. Jalali, "Self-phase-modulation induced spectral broadening in silicon waveguides," *Opt. Express*, vol. 12, no. 5, pp. 829–834, Mar. 2004.

[15] J. Zhang, Q. Lin, G. Piredda, R. W. Boyd, G. P. Agrawal, and P. M. Fauchet, "Optical solitons in a silicon waveguide," *Opt. Express*, vol. 15, no. 12, pp. 7682–7688, Jun. 2007.

[16] E. Dulkeith, Y. A. Vlasov, X. Chen, N. C. Panoiu, and R. M. Osgood, Jr., "Self-phase-modulation in submicron silicon-on-insulator photonic wires," *Opt. Express*, vol. 14, no. 12, pp. 5524–5534, Jun. 2006.

[17] R. Dekker, A. Driessen, T. Wahlbrink, C. Moormann, J. Niehusmann, and M. Först, "Ultrafast Kerr-induced all-optical wavelength conversion in silicon waveguides using 1.55 μm femtosecond pulses," *Opt. Express*, vol. 14, no. 18, pp. 8336–8346, Sep. 2006.

[18] D. J. Moss, L. Fu, I. Littler, and B. J. Eggleton, "Ultrafast all-optical modulation via two-photon absorption in silicon-on-insulator waveguides," *Electron. Lett.*, vol. 41, no. 6, pp. 320–321, Mar. 2005.

[19] E. K. Tien, N. S. Yuksek, F. Qian, and O. Boyraz, "Pulse compression and modelocking by using TPA in silicon waveguides," *Opt. Express*, vol. 15, no. 10, pp. 6500–6506, May 2007.

[20] T. K. Liang, L. R. Nunes, M. Tsuchiya, K. S. Abedin, T. Miyazaki, D. Van Thourhout, W. Bogaerts, P. Dumon, R. Baets, and H. Tsang, "High speed logic gate using two-photon absorption in silicon waveguides," *Opt. Commun.*, vol. 265, no. 1, pp. 171–174, Sep. 2006.

[21] T. Liang, L. Nunes, T. Sakamoto, K. Sasagawa, T. Kawanishi, M. Tsuchiya, G. Priem, D. Van Thourhout, P. Dumon, R. Baets, and H. Tsang, "Ultrafast all-optical switching by cross-absorption modulation in silicon wire waveguides," *Opt. Express*, vol. 13, no. 19, pp. 7298–7303, Sep. 2005.

[22] M. W. Geis, S. J. Spector, R. C. Williamson, and T. M. Lyszczarz, "Submicrosecond submilliwatt silicon-on-insulator thermooptic switch," *IEEE Photon. Technol. Lett.*, vol. 16, no. 11, pp. 2514–2516, Nov. 2004.

[23] H. Rong, A. Liu, R. Jones, O. Cohen, D. Hak, R. Nicolaescu, A. Fang, and M. Paniccia, "An all-silicon Raman laser," *Nature*, vol. 433, no. 7023, pp. 292–294, Jan. 2005.

[24] H. Rong, R. Jones, A. Liu, O. Cohen, D. Hak, A. Fang, and M. Pannicia, "A continuous-wave Raman silicon laser," *Nature*, vol. 433, no. 7027, pp. 725–728, Feb. 2005.

[25] O. Boyraz and B. Jalali, "Demonstration of directly modulated silicon Raman laser," *Opt. Express*, vol. 13, no. 3, pp. 796–800, Feb. 2005.
[26] O. Boyraz and B. Jalali, "Demonstration of a silicon Raman laser," *Opt. Express*, vol. 12, no. 21, pp. 5269–5273, Oct. 2004.
[27] M. Krause, H. Renner, and E. Brinkmeyer, "Analysis of Raman lasing characteristics in silicon-on-insulator waveguides," *Opt. Express*, vol. 12, no. 23, pp. 5703–5710, Nov. 2004.
[28] Q. Lin, J. Zhang, P. M. Fauchet, and G. P. Agrawal, "Ultrabroadband parametric generation and wavelength conversion in silicon waveguides," *Opt. Express*, vol. 14, no. 11, pp. 4786–4799, May 2006.
[29] H. Rong, Y. H. Kuo, A. Liu, M. Paniccia, and O. Cohen, "High efficiency wavelength conversion of 10 Gb/s data in silicon waveguides," *Opt. Express*, vol. 14, no. 3, pp. 1182–1188, Feb. 2006.
[30] R. L. Espinola, J. I. Dadap, R. M. Osgood, Jr., S. J. McNab, and Y. A. Vlasov, "C-band wavelength conversion in silicon photonic wire waveguides," *Opt. Express*, vol. 13, no. 11, pp. 4341–4349, May 2005.
[31] V. Raghunathan, R. Claps, D. Dimitropoulos, and B. Jalali, "Parametric Raman wavelength conversion in scaled silicon waveguides," *J. Lightw. Technol.*, vol. 23, no. 6, pp. 2094–2102, Jun. 2005.
[32] R. Claps, V. Raghunathan, D. Dimitropoulos, and B. Jalali, "Anti-Stokes Raman conversion in silicon waveguides," *Opt. Express*, vol. 11, no. 22, pp. 2862–2872, Nov. 2003.
[33] R. Jones, H. Rong, A. Liu, A. W. Fang, M. J. Paniccia, D. Hak, and O. Cohen, "Net continuous-wave optical gain in a low loss silicon-on-insulator waveguide by stimulated Raman scattering," *Opt. Express*, vol. 13, no. 2, pp. 519–525, Jan. 2005.
[34] A. Liu, H. Rong, M. Paniccia, O. Cohen, and D. Hak, "Net optical gain in a low loss silicon-on-insulator waveguide by stimulated Raman scattering," *Opt. Express*, vol. 12, no. 18, pp. 4261–4268, Sep. 2004.
[35] O. Boyraz and B. Jalali, "Demonstration of 11 dB fiber-to-fiber gain in a silicon Raman amplifier," *IEICE Electron. Express*, vol. 1, no. 14, pp. 429–434, Oct. 2004.
[36] R. Espinola, J. Dadap, R. M. Osgood, Jr., S. J. McNab, and Y. A. Vlasov, "Raman amplification in ultrasmall silicon-on-insulator wire waveguides," *Opt. Express*, vol. 12, no. 16, pp. 3713–3718, Aug. 2004.
[37] R. Claps, D. Dimitropoulos, V. Raghunathan, Y. Han, and B. Jalali, "Observation of stimulated Raman amplification in silicon waveguides," *Opt. Express*, vol. 11, no. 15, pp. 1731–1739, Jul. 2003.
[38] R. Jones, A. Liu, H. Rong, M. Paniccia, O. Cohen, and D. Hak, "Lossless optical modulation in a silicon waveguide using stimulated Raman scattering," *Opt. Express*, vol. 13, no. 5, pp. 1716–1723, Mar. 2005.
[39] W. Ding, C. Benton, A. V. Gorbach, W. J. Wadsworth, J. C. Knight, D. V. Skryabin, M. Gnan, M. Sorrel, and R. M. De La Rue, "Solitons and spectral broadening in long silicon-on-insulator photonic wires," *Opt. Express*, vol. 16, no. 5, pp. 3310–3319, Mar. 2008.
[40] I.-W. Hsieh, X. Chen, J. I. Dadap, N. C. Panoiu, and R. M. Osgood, Jr., "Cross-phase modulation-induced spectral and temporal effects on co-propagating femtosecond pulses in silicon photonic wires," *Opt. Express*, vol. 15, no. 3, pp. 1135–1146, Feb. 2007.
[41] I.-W. Hsieh, X. Chen, J. I. Dadap, N. C. Panoiu, R. M. Osgood, Jr., S. J. McNab, and Y. A. Vlasov, "Ultrafast-pulse self-phase modulation and third-order dispersion in Si photonic wire-waveguides," *Opt. Express*, vol. 14, no. 25, pp. 12 380–12 387, Dec. 2006.
[42] T. K. Liang and H. K. Tsang, "Nonlinear absorption and Raman scattering in silicon-on-insulator optical waveguides," *IEEE J. Sel. Topics Quantum Electron.*, vol. 10, no. 5, pp. 1149–1153, Sep./Oct. 2004.
[43] G. W. Rieger, K. S. Virk, and J. F. Yong, "Nonlinear propagation of ultrafast 1.5 μm pulses in high-index-contrast silicon-on-insulator waveguides," *Appl. Phys. Lett.*, vol. 84, no. 6, pp. 900–902, Feb. 2004.
[44] S. Afshar V. and T. M. Monro, "A full vectorial model for pulse propagation in emerging waveguides with subwavelength structures part I: Kerr nonlinearity," *Opt. Express*, vol. 17, no. 4, pp. 2298–2318, Feb. 2009.
[45] N. Suzuki, "FDTD analysis of two-photon absorption and free-carrier absorption in Si high-index-contrast waveguides," *J. Lightw. Technol.*, vol. 25, no. 9, pp. 2495–2501, Sep. 2007.
[46] G. P. Agrawal, *Nonlinear Fiber Optics*. Boston, MA: Academic, 2007.
[47] L. Yin, Q. Lin, and G. P. Agrawal, "Dispersion tailoring and soliton propagation in silicon waveguides," *Opt. Lett.*, vol. 31, no. 9, pp. 1295–1297, May 2006.
[48] V. M. N. Passaro and F. De Leonardis, "Space-time modeling of Raman pulses in silicon-on-insulator optical waveguides," *J. Lightw. Technol.*, vol. 24, no. 7, pp. 2920–2931, Jul. 2006.
[49] X. Chen, N. C. Panoiu, and R. M. Osgood, Jr., "Theory of Raman-mediated pulsed amplification in silicon-wire waveguides," *IEEE J. Quantum Electron.*, vol. 42, no. 2, pp. 160–170, Feb. 2006.
[50] D. Dimitropoulos, B. Houshmand, R. Claps, and B. Jalali, "Coupled-mode theory of Raman effect in silicon-on-insulator waveguides," *Opt. Lett.*, vol. 28, no. 20, pp. 1954–1956, Oct. 2003.
[51] I. D. Rukhlenko, M. Premaratne, and G. P. Agrawal, "Analytical study of optical bistability in silicon ring resonators," *Opt. Lett.*, vol. 35, no. 1, pp. 55–57, Jan. 2010.
[52] I. D. Rukhlenko, M. Premaratne, and G. P. Agrawal, "Analytical study of optical bistability in silicon-waveguide resonators," *Opt. Express*, vol. 17, no. 24, pp. 22 124–22 137, Nov. 2009.
[53] L. Yin, J. Zhang, P. M. Fauchet, and G. P. Agrawal, "Optical switching using nonlinear polarization rotation inside silicon waveguides," *Opt. Lett.*, vol. 34, no. 4, pp. 476–478, Feb. 2009.
[54] I. D. Rukhlenko, M. Premaratne, C. Dissanayake, and G. P. Agrawal, "Nonlinear pulse evolution in silicon waveguides: An approximate analytic approach," *J. Lightw. Technol.*, vol. 27, no. 15, pp. 3241–3248, Aug. 2009.
[55] I. D. Rukhlenko, M. Premaratne, C. Dissanayake, and G. P. Agrawal, "Continuous-wave Raman amplification in silicon waveguides: Beyond the undepleted pump approximation," *Opt. Lett.*, vol. 34, no. 4, pp. 536–538, Feb. 2009.
[56] I. D. Rukhlenko, C. Dissanayake, M. Premaratne, and G. P. Agrawal, "Maximization of net optical gain in silicon-waveguide Raman amplifiers," *Opt. Express*, vol. 17, no. 7, pp. 5807–5814, Mar. 2009.
[57] J. Y. Lee, L. Yin, G. P. Agrawal, and P. M. Fauchet, "Ultrafast optical switching based on nonlinear polarization rotation in silicon waveguides," *Opt. Express*, vol. 18, 2010.

[58] R. H. Stolen, J. Botineau, and A. Ashkin, "Intensity discrimination of optical pulses with birefringent fibers," *Opt. Lett.*, vol. 7, no. 10, pp. 512–514, Oct. 1982.
[59] D.-X. Xu, P. Cheben, D. Dalacu, A. Delâge, S. Janz, B. Lamontagne, M.-J. Picard, and W. N. Ye, "Eliminating the birefringence in silicon-on-insulator ridge waveguides by use of cladding stress," *Opt. Lett.*, vol. 29, no. 20, pp. 2384–2386, Oct. 2004.
[60] B. S. Gopalakrishnapillai, M. Premaratne, A. Nirmalathas, and C. Lim, "Power equalization using polarization rotation in semiconductor optical amplifiers," *IEEE Photon. Technol. Lett.*, vol. 17, no. 8, pp. 1695–1697, Aug. 2005.